

RESEARCH ARTICLE

The PRDM14–CtBP1/2–PRC2 complex regulates transcriptional repression during the transition from primed to naïve pluripotency

Maiko Yamamoto^{1,‡}, Yoshiaki Suwa^{1,‡}, Kohta Sugiyama^{1,‡}, Naoki Okashita^{1,*}, Masanori Kawaguchi¹, Naoki Tani², Kazumi Matsubara¹, Akira Nakamura³ and Yoshiyuki Seki^{1,§}

ABSTRACT

The pluripotency-associated transcriptional network is regulated by a core circuitry of transcription factors. The PR domain-containing protein PRDM14 maintains pluripotency by activating and repressing transcription in a target gene-dependent manner. However, the mechanisms underlying dichotomic switching of PRDM14-mediated transcriptional control remain elusive. Here, we identified C-terminal binding protein 1 and 2 (CtBP1 and CtBP2; generically referred to as CtBP1/2) as components of the PRDM14-mediated repressive complex. CtBP1/2 binding to PRDM14 depends on CBFA2T2, a core component of the PRDM14 complex. The loss of *Ctbp1/2* impaired the PRDM14-mediated transcriptional repression required for pluripotency maintenance and transition from primed to naïve pluripotency. Furthermore, CtBP1/2 interacted with the PRC2 complexes, and the loss of *Ctbp1/2* impaired Polycomb repressive complex 2 (PRC2) and H3K27me3 enrichment at target genes after *Prdm14* induction. These results provide evidence that the target gene-dependent transcriptional activity of PRDM14 is regulated by partner switching to ensure the transition from primed to naïve pluripotency.

This article has an associated First Person interview with the first author of the paper

KEY WORDS: PRDM14–CtBP1/2–PRC2 complex, Transcriptional repression, Pluripotency, Embryonic stem cells

INTRODUCTION

Pluripotent cells are common sources of germline and somatic cells. They are established early in the mammalian embryo. Cellular pluripotency is governed by core transcriptional regulatory circuitry centered on POU5F1 (also known as OCT4) and NANOG (Niwa, 2014). During embryogenesis, *Pou5f1* expression in the inner cell mass (ICM) of the blastocyst is maintained in the epiblast and primordial germ cells (PGCs). In contrast, naïve pluripotent

markers, such as *Nanog*, *Prdm14* and *Klf2*, are repressed during the transition from ICM to epiblast cells. PRDM14 is a sequence-specific transcriptional regulator. Somatic cells maintain *Prdm14* repression. Primordial germ cells (PGCs) specified from most proximal epiblast cells are associated with the reactivation of *Prdm14* expression. This process is necessary for PGC formation (Yamaji et al., 2008; Nakaki et al., 2013). PGCs are specified by the activation of pluripotency-associated genes, the repression of epiblast markers and epigenetic reprogramming regulated by repressing major enzymes that methylate DNA and H3K9 (Kurimoto et al., 2008; Seki et al., 2007; Ohno et al., 2013; Kagiwada et al., 2013). We previously showed that PRDM14 induction in epiblast-like cells activates pluripotency-associated genes (*Klf2*, *Tcl1* and *Tfcp2l1*) and represses epiblast markers (*Otx2*, *Dnmt3b* and *Fgf5*). Thus, PRDM14 can both activate and repress transcription depending on the target genes (Okashita et al., 2016). The activation of pluripotent-associated genes by PRDM14 depends on OCT4 recruitment through TET-mediated DNA demethylation. However, the mechanism by which PRDM14 represses epiblast markers remains unknown (Seki, 2018).

A knockout (KO) study has previously shown that PRDM14 shuts off autocrine fibroblast growth factor (FGF) signaling (a crucial differentiation trigger) to maintain mouse embryonic stem cell (mESC) pluripotency through the transcriptional repression of *Fgfr1* and/or *Fgfr2* under serum plus leukemia inhibitory factor (LIF) (Yamaji et al., 2013). In the presence of the MEK and GSK-3 inhibitors (denoted ‘2i’), in addition to LIF, the self-renewal of *Prdm14*-deficient ESCs is maintained because of the repression of FGF signaling via the MEK inhibitor (MEKi). SUZ12, one of the Polycomb repressive complex 2 (PRC2) components, is biotinylated by PRDM14 and biotin ligase, which indicates that PRC2 is localized near PRDM14 in the nucleus of ESCs. The loss of *Prdm14* reduces PRC2 and H3K27me3 enrichment at target genes such as *Dnmt3b* and *Fgfr1* and *Fgfr2*. Previous studies have not described the biochemical purification of the components of the PRC2 complex with PRDM14 using immunoprecipitation analysis from ESC nuclear lysates (Nady et al., 2015; Tu et al., 2016). Instead, a co-repressor protein CBFA2T2 was identified as a core component of the PRDM14 complex. CBFA2T2 directly interacts with PRDM14 to form a scaffold that stabilizes PRDM14 on the chromatin and regulates target gene transcription and repression. The *Cbfa2t2* KO phenotypes are nearly identical to those of *Prdm14* KO in ESC and PGC development. These findings demonstrate that CBFA2T2 is an essential component of the PRDM14 complex for both transcriptional activation and repression. However, how dichotomic switching of the target gene-dependent transcriptional activity of PRDM14 is operated remains unknown.

Here, we investigated the N-terminal domain of PRDM14, which has no discernible functional domain, and its contribution to the

¹Department of Biomedical Chemistry, School of Science and Technology, Kwansai Gakuin University, 2-1 Gakuen, Sanda, Hyogo 669-1337, Japan. ²Liaison Laboratory Research Promotion Center, Institute of Molecular Embryology and Genetics, Kumamoto University, 2-2-1 Honjo, Chuo-ku, Kumamoto 860-0811, Japan. ³Department of Germline Development, Institute of Molecular Embryology and Genetics, Kumamoto University, 2-2-1 Honjo, Chuo-ku, Kumamoto 860-0811, Japan.

*Present address: Laboratory of Epigenome Dynamics, Graduate School of Frontier Biosciences, Osaka University, 1-3 Yamadaoka, Suita, Osaka 565-0871, Japan.

[‡]These authors contributed equally to this work

[§]Author for correspondence (yseki@kwansai.ac.jp)

 A.N., 0000-0001-6506-9146; Y.S., 0000-0001-5745-5549

Handling Editor: Maria Carmo-Fonseca
Received 27 November 2019; Accepted 25 June 2020

maintenance of pluripotency. We performed a mass spectrometry analysis of the PRDM14-containing complex to disclose partner molecules that bind to the N-terminal domain of PRDM14. Knockout models of *Ctbp1/2*, *Suz12* and *Cbfa2t2* were employed to delineate possible interactions between CTBP1/2 and the PRDM14–CBFA2T2 complex with PRC2 at repressed target genes in ESCs.

RESULTS

Functional domain mapping of PRDM14

Several studies have demonstrated that PRDM14 controls the transcriptional networks required for pluripotency. These include the self-renewal of ESCs cultured in serum plus LIF (Yamaji et al., 2013), LIF-independent self-renewal of ESCs (Okashita et al., 2015), and conversion from epiblast-like cells (EpiLCs) to ESCs

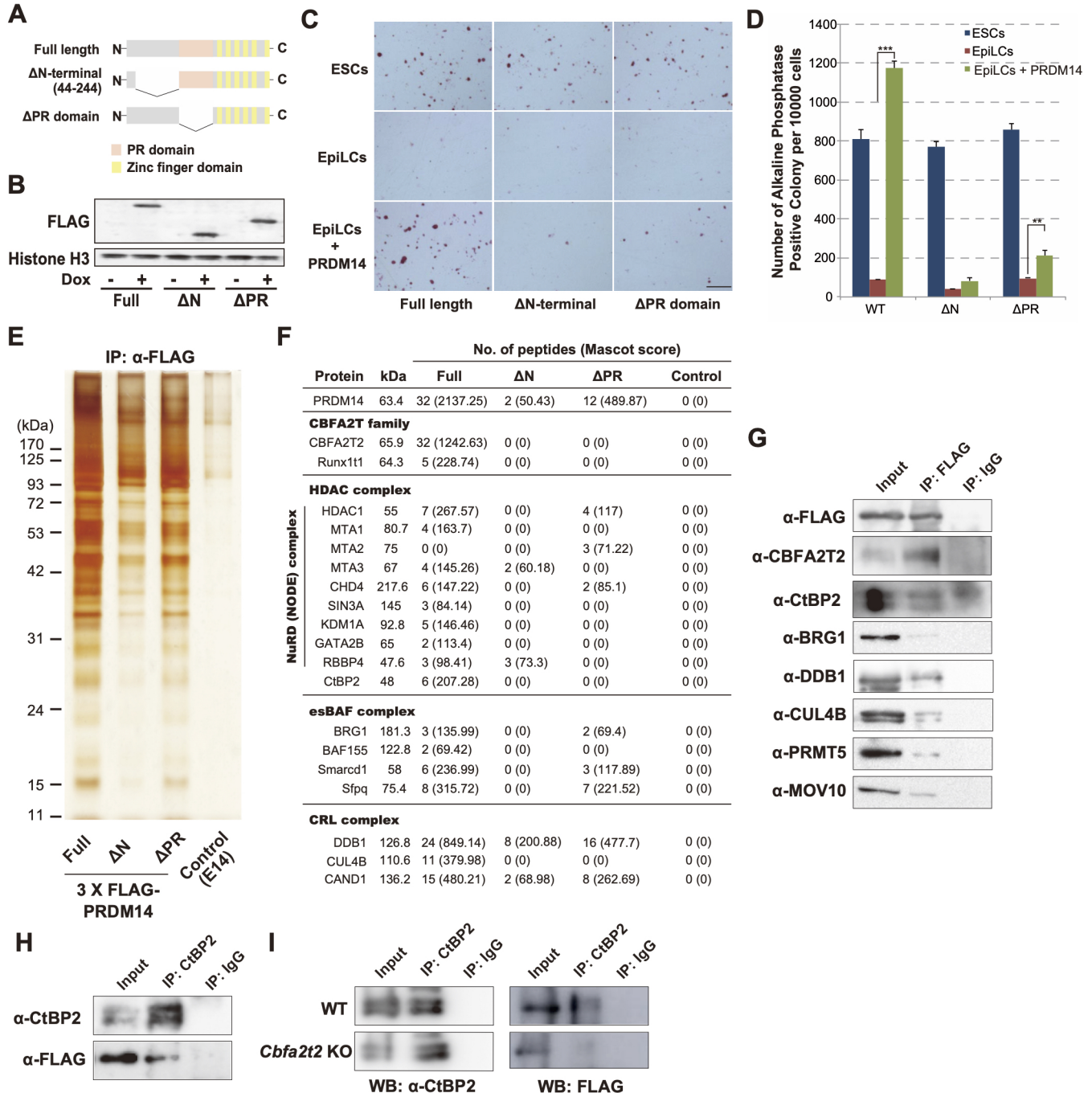


Fig. 1. PRDM14 interacts with CtBP2 through CBFA2T2. (A) Diagram of full-length and deletion mutant of PRDM14 used here. (B) The protein expression of full-length and deletion mutant of PRDM14 in ESCs with or without doxycycline as assessed by western blotting. (C,D) AP staining of ESCs and EpiLCs with or without exogenous *Prdm14* expression cultured in serum plus LIF for 3 days. Results are mean \pm s.e.m. of biological triplicates. $**P < 0.01$, $***P < 0.001$ (Tukey–Kramer multiple comparisons test). (E) Silver staining of immunoprecipitants from whole-cell extracts of full-length, and N-terminal and PR domain deletions of PRDM14 in ESCs after *Prdm14* induction. (F) MS of peptide counts for full-length, and N-terminal and PR domain deletions of PRDM14 in ESCs. Results in E and F are representative of two experiments. (G) Immunoprecipitation with antibody against FLAG–PRDM14 from whole-cell lysates of ESCs cultured in serum plus LIF after *Prdm14* induction, followed by western blotting with antibodies against indicated proteins. (H,I) Immunoprecipitation with anti-CtBP2 antibody from whole-cell lysates of wild-type (WT) or *Cbfa2t2* KO ESCs cultured in 2i plus LIF after *Prdm14* induction. Results in G–I are representative of two experiments.

(Okashita et al., 2016) (Fig. S1A). To elucidate the functional domains of PRDM14 that regulate mESC pluripotency, we established a doxycycline-inducible expression system of full-length PRDM14 and PRDM14 mutants lacking the N-terminal or PR domain in *Prdm14*-deficient mESCs (Fig. 1A; Fig. S1B). In the absence of doxycycline, and hence *Prdm14* expression, cell lines could not expand beyond four passages over 8 days in serum plus LIF (Fig. S1C,D). This observation was consistent with a previous report (Yamaji et al., 2013). *Prdm14*-deficient mESCs expressing exogenous full-length PRDM14 could expand and retain alkaline phosphatase activity in the serum plus LIF condition. Deletion of the N-terminal domain of PRDM14 completely eliminated the maintenance of mESC pluripotency, whereas PRDM14 without PR domain expression partially supported the self-renewal activity of *Prdm14*-deficient mESCs in serum plus LIF. To analyze the functional domains of PRDM14 in LIF-independent self-renewal of ESCs with PRDM14 overexpression (Okashita et al., 2015), we created ESCs in which full-length PRDM14 and PRDM14 mutants lacking N-terminal- or PR domain are induced by doxycycline administration (Fig. 1A,B). Overexpression of full-length PRDM14 in ESCs maintained alkaline phosphatase (AP) activity in the absence of LIF, while the maintenance of pluripotency was diminished by the deletion of N-terminal or PR domain (Fig. S1E). ESCs can be differentiated into epiblast-like cells (EpiLCs) by stimulation with Activin A, bFGF and 1% knockout serum replacement (SR), and this is associated with the downregulation of pluripotency-associated factors and the upregulation of epiblast markers (Hayashi et al., 2011). Consistent with our previous study (Okashita et al., 2016), EpiLCs overexpressing full-length PRDM14 retained the AP activity in the serum plus LIF condition similar to what was seen for ESCs (Fig. 1C,D). However, the deletion of the N-terminal region or PR domain of PRDM14 significantly impaired the conversion efficiency from EpiLCs into ESCs. Thus, although the N-terminal region of PRDM14 does not have a discernible functional domain apparent in its primary sequence, it is essential for pluripotency induction and maintenance.

Identification of the components of PRDM14 complex in ESCs

We sought for components of PRDM14 complex by shotgun liquid chromatography-tandem mass spectrometry (LC-MS/MS). PRDM14 complex was immunopurified with anti-FLAG antibody from whole-cell lysates of ESCs expressing FLAG-PRDM14, FLAG-PRDM14 Δ N and FLAG-PRDM14 Δ PR cultured in serum plus LIF, and separated by SDS-PAGE. MS analysis of silver-stained immunoprecipitated proteins showed that the deletion of the N-terminal region of PRDM14 significantly reduced the number of proteins co-immunoprecipitated with PRDM14 (Fig. 1E). Consistent with a previous study (Nady et al., 2015; Tu et al., 2016), CBFA2T2 was found to be a major component of the PRDM14 complex (Fig. 1F). CBFA2T2 was detected in the full-length PRDM14 complex, but was absent in Δ N and Δ PR PRDM14 complexes, indicating that interaction between PRDM14 and CBFA2T2 depended on both the N-terminal region and the PR domain. MS analysis also identified proteins that are known components of the NODE, esBAF and CRL4 complexes, and CtBP2 (Liang et al., 2008; Ho et al., 2009a; Gao et al., 2015). Western blot analysis of PRDM14 immunoprecipitates confirmed the interaction of PRDM14 with the aforementioned molecules (Fig. 1G). Proximity-dependent biotin identification (BioID) methods have previously detected the interaction of PRDM14

with the components of PRC2 in ESCs (Yamaji et al., 2013). However, our immunoprecipitation assay using antibody against FLAG-PRDM14 followed by MS analysis did not detect the components of PRC2. Other researchers also failed to detect the components of PRC2 upon immunoprecipitation of PRDM14 complex followed by MS (Nady et al., 2015; Tu et al., 2016). This suggests that the interaction between PRDM14 and PRC2 components may be very weak, transient and/or indirect, such that the interaction could not be detected by the immunoprecipitation-MS strategy we used.

In this study, we focused on CtBP2 among the components of the PRDM14 complex because CtBP2 is reported to recruit the PRC2 complex at target genes (Kim et al., 2015). Immunoprecipitation of CtBP2 followed by western blotting with anti-FLAG antibody confirmed the interaction between CtBP2 and PRDM14 (Fig. 1H). LC-MS/MS of the PRDM14 complex indicated that, similar to the case for CBFA2T2, CtBP2 was present only with the full-length PRDM14 complex (Fig. 1F). Intriguingly, there were fewer peptides detected that matched CtBP2 compared with those matching CBFA2T2. Given that the latter is a direct stoichiometric partner of PRDM14 (Nady et al., 2015), PRDM14 might indirectly interact with CtBP2 via CBFA2T2 in ESCs. We therefore created *Cbfa2t2* KO ESCs carrying a doxycycline-inducible *Prdm14* expression unit to determine whether the interaction between PRDM14 and CtBP2 is CBFA2T2 dependent (Fig. S2A). As in the case of *Prdm14* KO ESCs, because *Cbfa2t2* KO ESCs could not be maintained in serum plus LIF condition (Tu et al., 2016), we screened for the interaction between PRDM14 and CtBP2 in ESCs lacking *Cbfa2t2* under the 2i plus LIF condition. PRDM14 also interacted with CtBP2 in wild-type ESCs, although the interaction of PRDM14 with CtBP2 was significantly impaired in the absence of *Cbfa2t2* (Fig. 1I). These results indicate that the PRDM14-CtBP2 interaction is CBFA2T2 dependent, suggesting that PRDM14 indirectly interacts with CtBP2 through CBFA2T2 in ESCs.

PRDM14 recruits CtBP2 at the repressive targets

To investigate whether PRDM14 and CtBP2 binding on the genome overlapped in mESCs, we reconstructed chromatin immunoprecipitation (ChIP)-seq tag mapping for PRDM14 and CtBP2 near the PRDM14-binding regions using published datasets (Kim et al., 2015; Ma et al., 2011). We found that over 50% of CtBP2-binding peaks were enriched and overlapped with the PRDM14-binding peaks in mESCs (Fig. 2A,B). To examine whether the CtBP2 recruitment at PRDM14 target genes (*Dnmt3b*, *Zfp281* and *Id1*) (Fig. 2C) depended on PRDM14, we used ChIP-qPCR to compare the PRDM14 and CtBP2 enrichments at these genes before and after *Prdm14* induction under the serum plus LIF condition (Fig. 2D). At 2 days after *Prdm14* induction, FLAG-PRDM14 was significantly enriched at loci of all the genes, and CtBP2 and HDAC1 enrichments to these loci were also upregulated. In contrast, H3 lysine acetylation (H3KAc) was decreased by *Prdm14* induction at all loci. These results show that the recruitment of the CtBP2-HDAC1 repressive complex at these repressive target genes is PRDM14 dependent.

We have previously shown that PRDM14 overexpression reduces promoter cytosine methylation of pluripotency-associated- and germline-specific genes through the recruitment of ten-eleven translocation (TET) proteins, resulting in upregulation of these target genes (Okashita et al., 2014). To investigate the switching of PRDM14 complexes in the target-dependent manners, we compared CtBP2 enrichment before and after *Prdm14* induction at pluripotency-associated- and germline-specific genes. Publicly accessible ChIP-seq data showed that CtBP2 was not colocalized

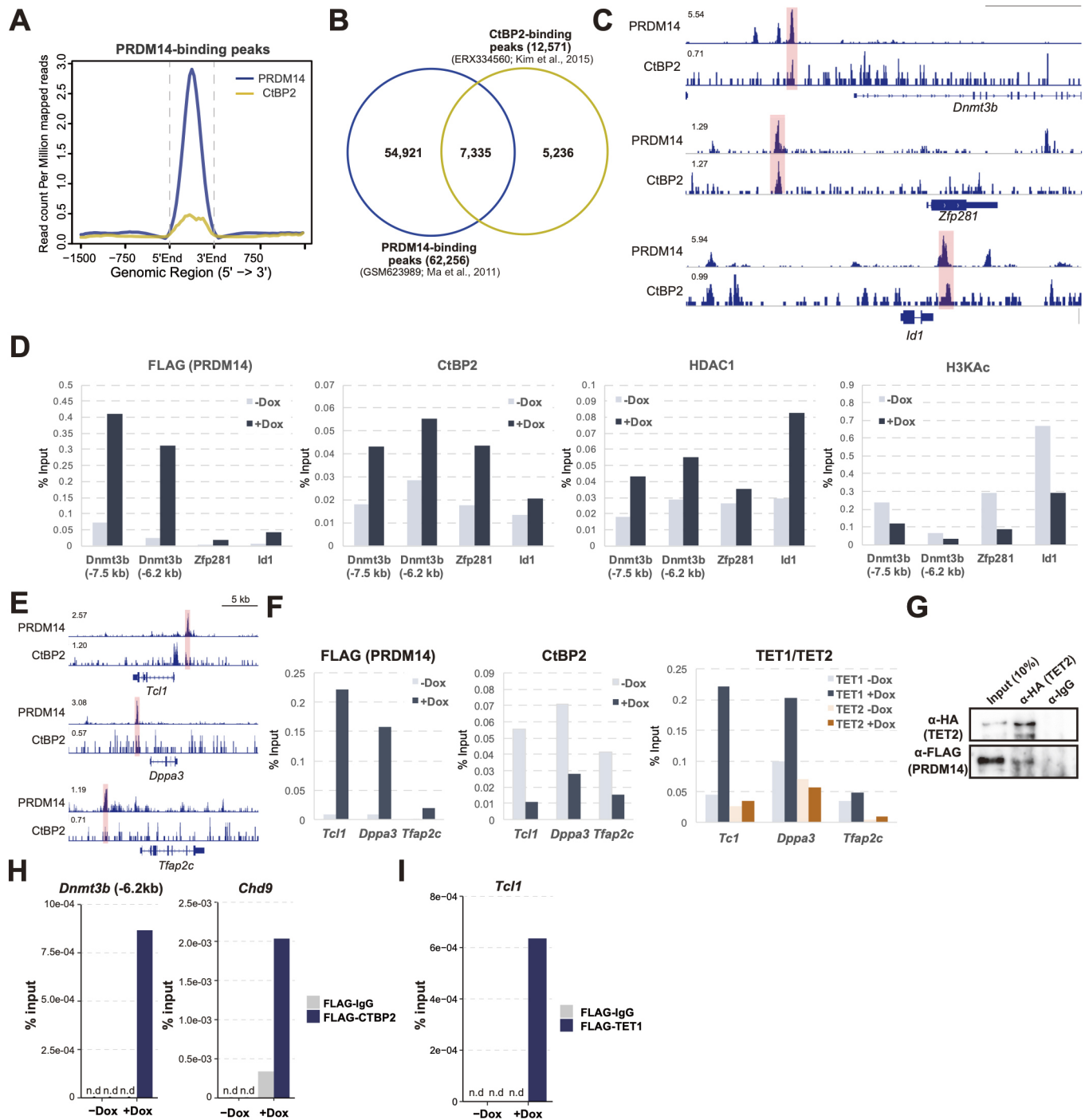


Fig. 2. PRDM14 recruits CtBP2 at repressive but not active targets. (A) Histogram showing enrichment of PRDM14- and CtBP2-binding peaks near PRDM14-binding regions in ESCs (Ma et al., 2011; GSM623989), (Kim et al., 2015; ERX334560). (B) Venn diagram showing overlapping PRDM14- and CtBP2-binding peaks (Ma et al., 2011; GSM623989), (Kim et al., 2015; ERX334560). (C) Gene tracks showing that PRDM14-binding peaks colocalized with CtBP2 at repressive PRDM14 targets (Ma et al., 2011; GSM623989), (Kim et al., 2015; ERX334560). (D) ChIP-qPCR of PRDM14, CtBP2, HDAC1 and H3KAc before and after *Prdm14* induction. (E) Gene tracks showing that PRDM14-binding peaks did not colocalize with CtBP2 at active PRDM14 targets (Ma et al., 2011; GSM623989), (Kim et al., 2015; ERX334560). (F) ChIP-qPCR of PRDM14, CtBP2 and TET1/TET2 before and after *Prdm14* induction at active PRDM14 targets. (G) Pull-down of recombinant HA-TET2 protein with recombinant FLAG-PRDM14 followed by western blotting with anti-HA or anti-FLAG antibodies. Results are representative of two experiments. (H,I) Sequential ChIP (re-ChIP) was performed by initial immunoprecipitation with FLAG antibody followed by CtBP2 (H) and (I) TET1 antibody, respectively. n.d. indicates non detection of qPCR amplification curves.

with PRDM14 at *Tcl1*, *Dppa3* and *Tfap2c* (Fig. 2E). Unlike the repressive target genes, CtBP2 enrichment was significantly decreased by *Prdm14* induction, whereas TET1 enrichment was consistently increased by *Prdm14* induction at *Tcl1*, *Dppa3* and

Tfap2c (Fig. 2F). Contrary to the interaction of PRDM14 with CtBP2 through CBFA2T2, pull-down assay using the recombinant proteins FLAG-PRDM14 and HA-TET2 showed that PRDM14 directly interacted with TET2 in the absence of CBFA2T2

(Fig. 2G). Further, we performed a sequential ChIP for PRDM14 followed by CtBP2 or TET1, and showed that PRDM14 and CtBP2 or TET1 co-occupied target genes (Fig. 2H,I). These findings demonstrate that the recruitment PRDM14 partners on target genes varied between activating and repressing loci, suggesting that differences in the compositions of PRDM14 complexes on each target gene may account for dichotomic transcriptional switch of PRDM14.

PRC2 is required for PRDM14-dependent transcriptional repression

To establish whether CtBP2 mediates PRDM14 recruitment of the PRC2 complex, we compared H3K27me3 distribution

near the PRDM14- and CtBP2-binding regions and the PRDM14–CtBP2 co-binding region in ESCs using published ChIP-seq datasets (Ma et al., 2011; Kim et al., 2015; Ji et al., 2015). The H3K27me3 levels near the PRDM14-binding regions was significantly lower than those near the CtBP2-binding regions. However, the H3K27me3 levels near the PRDM14–CtBP2 co-binding regions were substantially higher than those near the CtBP2-binding regions (Fig. 3A). These results suggest that PRDM14 and CtBP2 coordinately regulate H3K27me3 levels at the silenced genes in mESCs, presumably by recruiting the PRC2 complex that methylates H3K27.

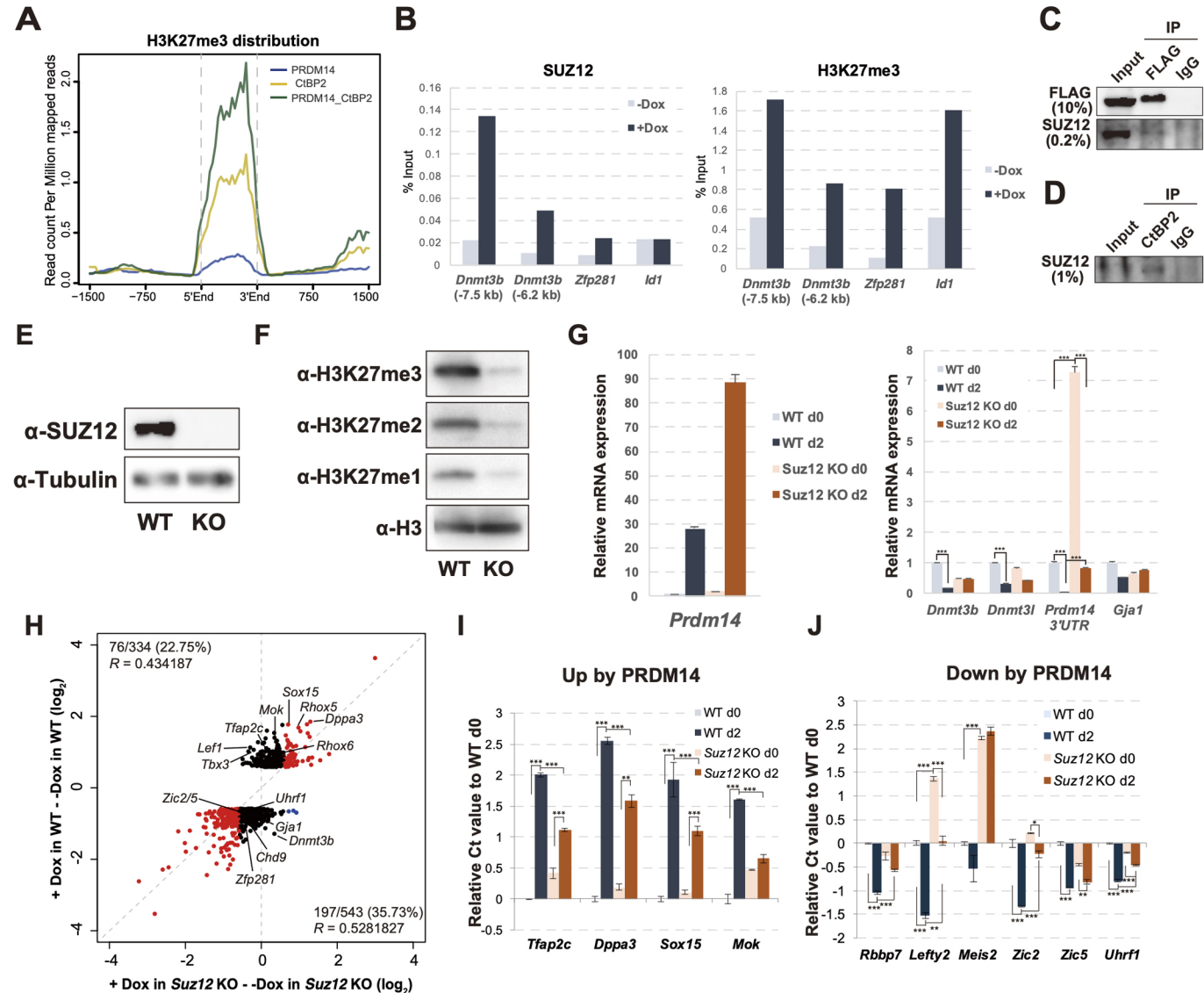


Fig. 3. Suz12 is partially involved in transcriptional PRDM14 repression in ESCs. (A) Histogram shows H3K27me3 enrichment near PRDM14- and CtBP2-binding peaks and PRDM14- and CtBP2-colocalized peaks in ESCs (Ma et al., 2011; GSM623898), (Kim et al., 2015; ERX334560), (Ji et al., 2015; GSM1526291). (B) ChIP-qPCR of SUZ12 and H3K27me3 before and after *Prdm14* induction at repressive targets of PRDM14. (C,D) Immunoprecipitation using antibodies against FLAG or CtBP2 followed by western blotting with indicated antibodies. (E,F) Western blot with anti-SUZ12, tubulin, histone H3, and H3K27me1/2/3 antibodies in wild-type (WT) and *Suz12* KO ESCs. Results in C and D are representative of two experiments. Results in E and F are representative of three experiments. (G) qRT-PCR of indicated genes in wild-type and *Suz12* KO ESCs before and after *Prdm14* induction. Results are mean±s.e.m. of biological triplicates. ****P*<0.001 (Tukey–Kramer multiple comparisons test). (H) Scatterplot of microarray data showing relative intensities of genes upregulated or downregulated by PRDM14 in wild-type and *Suz12* KO ESCs. Blue dots indicate genes downregulated by PRDM14 in wild-type ESCs and upregulated by PRDM14 in *Suz12* KO ESCs. *R* is the correlation coefficient. (I,J) qRT-PCR of indicated genes in wild-type and *Suz12* KO ESCs before and after *Prdm14* induction. Results are mean±s.e.m. of biological triplicates. ***P*<0.01, ****P*<0.001 (Tukey–Kramer multiple comparisons test).

To determine whether PRDM14 recruits the PRC2 complex at the target genes, we compared SUZ12, a central component of PRC2 and H3K27me3 enrichment at the target gene levels before and after *Prdm14* induction in mESCs under serum plus LIF condition. At 2 days after *Prdm14* induction, SUZ12 and H3K27 were consistently elevated at the target genes, except for *Id1* (Fig. 3B). Co-immunoprecipitation analysis disclosed a weak interaction between PRDM14 and SUZ12 (Fig. 3C). Consistent with a previous study, we found a more efficient co-immunoprecipitation of SUZ12 with CtBP2 (Fig. 3D). Therefore, PRDM14 appears to recruit the PRC2 complex at target genes mediated by CtBP2.

To elucidate the function of PRC2 in transcriptional regulation by PRDM14, we used a CRISPR/Cas9 system to create *Suz12* KO ESCs with the doxycycline-dependent *Prdm14* expression. We used a frameshift mutation to design a gRNA at exon 6 of the *Suz12* genomic region and delete the zinc finger domain located at the C-terminal region (Fig. S2B). Western blot analysis showed complete deletion of the SUZ12 proteins and significant reduction of genome-wide H3K27 methylation in *Suz12* KO ESCs (Fig. 3E,F). Comparison of the PRDM14-downregulated genes between the wild-type and *Suz12* KO ESCs indicated that repression of *Dnmt3l*, *Dnmt3b* and *Gja1* by PRDM14 was significantly impaired in *Suz12* KO ESCs (Fig. 3G). Furthermore, although *Prdm14* has negative-feedback activity and represses its own transcription in mESCs (Okashita et al., 2014), *Suz12* KO led to significantly upregulated endogenous *Prdm14*. Thus, SUZ12 is required for negative *Prdm14* feedback and/or active *Prdm14* repression by unknown factors in mESCs.

To analyze the global impact of *Suz12* KO in transcriptional PRDM14 regulation, we performed a microarray analysis to compare the effects of PRDM14 on relative gene expression in wild-type and *Suz12* KO ESCs. The PRDM14-mediated gene upregulation and downregulation observed in the wild-type ESCs were globally impaired in the *Suz12* KO (Fig. 3H). To confirm the results of microarray analysis, we performed qRT-PCR on selected genes (Fig. 3I,J). In *Suz12* KO ESCs, PRDM14-mediated upregulation of the early PGC markers was moderately impaired, whereas downregulation of the epiblast markers by PRDM14 was consistently disordered.

CtBP1/2 is partially required for PRDM14-mediated transcriptional repression

We used the CRISPR/Cas9 system to create *Ctbp2* single knockout and *Ctbp1/2* double knockout (DKO) ESCs with doxycycline-dependent *Prdm14* expression. We deleted the *Ctbp1* start codon and inserted the stop codon in *Ctbp2* (Fig. S2C). Consequently, these proteins were completely eliminated (Fig. 4A). *Ctbp2* deletion led to a flattening of the formerly dome-like mESC colonies (Fig. 4B). Immunofluorescence and western blotting analysis showed that the protein levels of OCT4 were maintained in *Ctbp1/2* DKO ESCs, as observed in wild-type ESCs (Fig. 4C,D). Wild-type ESCs showed a heterogeneous expression of NANOG, while it was homogeneous in *Ctbp1/2* DKO ESCs (Fig. 4C). Furthermore, the protein levels of NANOG was significantly elevated in *Ctbp1/2* DKO ESCs, suggesting that the loss of *Ctbp1/2* stabilizes the pluripotent network of transcription factors in ESCs under serum plus LIF condition (Fig. 4D). Next, we used microarray analysis to assess the impact of *Ctbp1/2* loss on PRDM14-mediated transcriptional regulation in ESCs by comparing expression levels between the wild-type and *Ctbp1/2* DKO ESCs. Unlike the *Suz12* KO phenotype, PRDM14-mediated transcriptional activation in

Ctbp1/2 DKO ESCs was relatively stable, whereas PRDM14-mediated transcriptional repression was significantly impaired (Fig. 4E,F). The results of the microarray analysis were corroborated by qRT-PCR (Fig. 4G). Unexpectedly, some early PGC markers (*Dppa3* and *Rhox6*) were significantly repressed in *Ctbp1/2* DKO ESCs. To determine whether CtBP2 participates in PRDM14-mediated repression of *Dnmt3b* transcription, we evaluated the effect of *Ctbp1/2* loss on *Dnmt3b* promoter activity regulated by PRDM14. *Dnmt3b* promoter activity was suppressed by PRDM14 expression in wild-type but not *Ctbp1/2* DKO ESCs (Fig. 4H). To clarify the hierarchy of PRDM14, CtBP2 and SUZ12 in PRDM14-mediated repression of *Dnmt3b* transcription, we compared PRDM14, SUZ12 and H3K27me3 enrichment on the *Dnmt3b* loci of wild-type and *Ctbp1/2* DKO ESCs before and after *Prdm14* induction. PRDM14 recruitment was significantly impaired by *Ctbp1/2* loss. In wild-type ESCs, SUZ12 and H3K27me3 enrichments were significantly elevated on the *Dnmt3b* loci after *Prdm14* induction, whereas they were completely abolished upon *Ctbp1/2* loss (Fig. 4I). Therefore, there is an absolute requirement for CtBP1/2 in the repression of *Dnmt3b* transcription by PRDM14 in ESCs.

SUZ12 is required for PRDM14-induced reversion from EpiLCs to ESCs

We have previously shown that PRDM14 overexpression converts EpiLCs into ESCs (Okashita et al., 2016). We therefore examined the role of the CtBP1/2-PRC2 axis in EpiLC to ESC conversion in response to PRDM14 overexpression. Before this process, ESCs must be cultured in 2i plus LIF medium to promote ground-state pluripotency (Hayashi et al., 2011). Unexpectedly, cell transfer from serum plus LIF to 2i plus LIF caused an abnormality in the *Ctbp1/2* KO ESCs growth rate as shown in Fig. 7A. Thus, we could not investigate the function of CtBP2 in the EpiLC experiments. To clarify the function of SUZ12 in PRDM14-associated pluripotency, we compared the conversion efficiency between wild-type and *Suz12* KO EpiLCs based on the number of AP-positive colonies, and found that PRDM14-induced transformation from EpiLCs to ESCs was significantly impaired in the *Suz12* KO background (Fig. 5A–D). RT-qPCR analysis showed that the activation of pluripotency-associated genes and the repression of differentiation markers were both diminished in *Suz12* KO (Fig. 5E,F). Thus, PRDM14 cooperates with SUZ12 to convert EpiLCs into ESCs by activating pluripotency-associated genes and repressing differentiation markers.

SUZ12-CtBP1/2 is required for transcriptional *Dnmt3b* and *Dnmt3l* repression in the ground state

Transfer of ESCs from serum plus LIF to 2i plus LIF upregulates *Prdm14* which, in turn, downregulates *Dnmt3a*, *Dnmt3b* and *Dnmt3l* (*Dnmt3a/b/l*) (Habibi et al., 2013). We determined whether *Suz12* and *Ctbp1/2* are required for the repression of *Dnmt3a/b/l* transcription during the transition from metastable- to ground-state pluripotency. Transfer of both wild-type and *Suz12* KO ESCs from serum plus LIF to 2i plus LIF produced the dome-shaped colonies characteristic of ground-state pluripotency associated with the elevation of *Prdm14* expression (Fig. 6A,C). AP activity was heterogeneous in wild-type and *Suz12* ESCs under the serum plus LIF condition, while ground-state ESCs derived from wild-type and *Suz12* KO ESCs showed homogeneous staining of AP activity (Fig. 6B). Contrary to the upregulation of *Prdm14*, *Dnmt3b* and *Dnmt3l* (*Dnmt3b/l*) repression was significantly diminished in *Suz12* KO ESCs in 2i plus LIF condition (Fig. 6C). In contrast, the

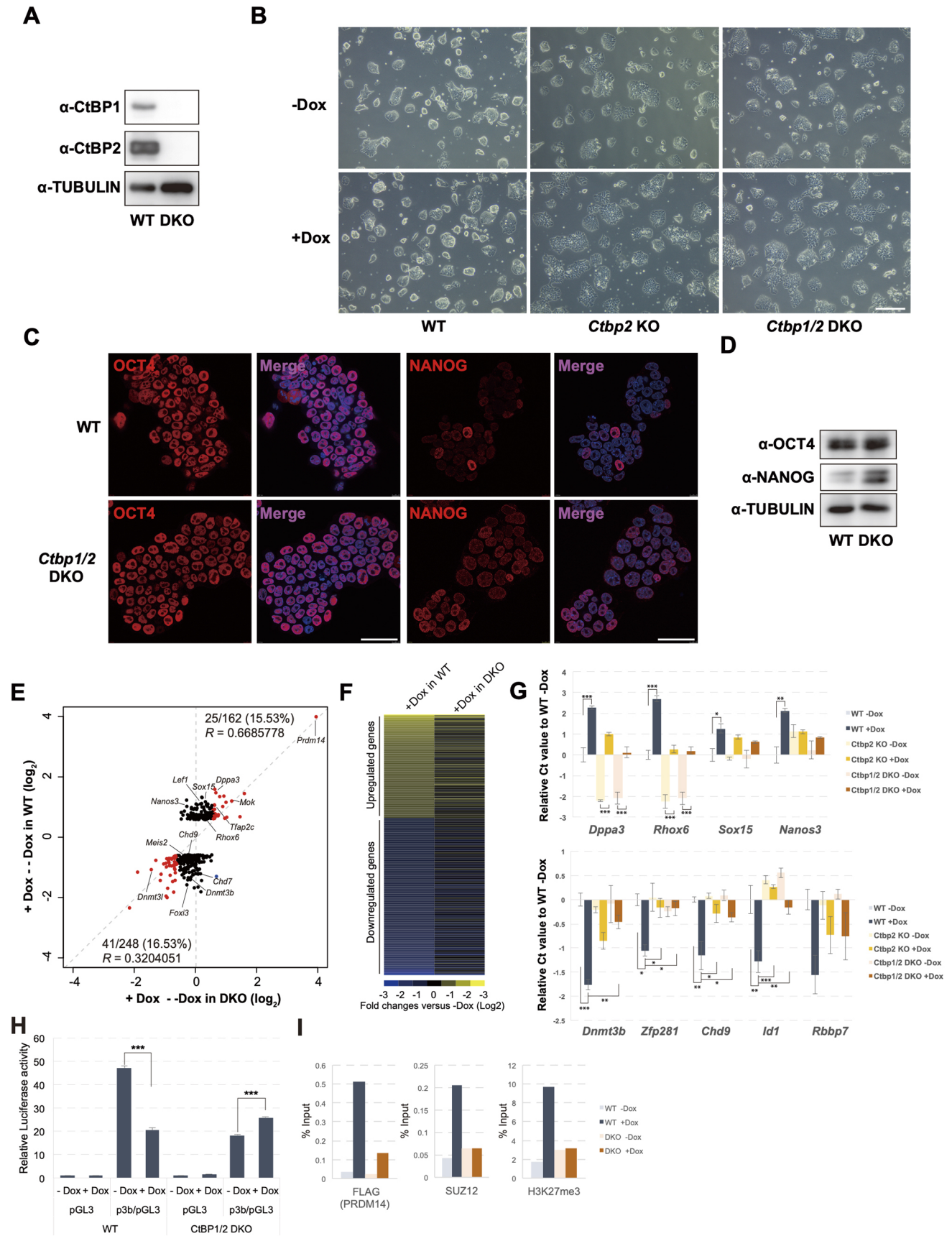


Fig. 4. See next page for legend.

Fig. 4. CtBP1/2 link PRDM14 to PRC2-mediated transcriptional repression.

(A) Western blot of indicated protein in wild-type (WT) and *Ctbp1/2* DKO ESCs. (B) Morphology of wild-type, *Ctbp2* KO and *Ctbp1/2* DKO ESCs before and after *Prdm14* induction. Scale bar: 50 μ m. (C) Immunofluorescence analysis of wild-type and *Ctbp1/2* DKO ESCs stained with anti-OCT4 or -NANOG antibody. Scale bars: 50 μ m. (D) Western blotting of wild-type and *Ctbp1/2* DKO ESCs with anti-OCT4, NANOG and tubulin antibody. Results in A–D are representative of two experiments. (E) Scatterplot of microarray data showing relative intensities of genes upregulated or downregulated by PRDM14 in wild-type and *Ctbp1/2* DKO ESCs. Red dots indicate genes either upregulated or downregulated by PRDM14 in both wild-type and *Suz12* KO ESCs. Blue dots indicate genes downregulated by PRDM14 in wild-type ESCs and upregulated by PRDM14 in *Ctbp1/2* KO ESCs. *R* is the correlation coefficient. (F) Heatmap showing relative expression levels (left column: +Dox vs –Dox in wild-type ESCs, right column: +Dox vs –Dox in *Ctbp1/2* DKO ESCs) of all differentially expressed genes either upregulated or downregulated by PRDM14 in wild-type ESCs. (G) qRT-PCR of indicated genes in wild-type and *Ctbp1/2* DKO ESCs before and after *Prdm14* induction. Results are mean \pm s.e.m. of biological triplicates. **P*<0.05, ***P*<0.01, ****P*<0.001 (Tukey–Kramer multiple comparisons test). (H) Luciferase assay on *Dnmt3b* locus in wild-type and *Ctbp1/2* DKO ESCs. pGL3 indicates pGL3-basic vector. p3b/pGL3 indicates pGL3-basic vector with the fragment of *Dnmt3b* locus (–8.6 kbp/+93 bp from the transcription start site). Results are mean \pm s.e.m. of biological triplicates. ****P*<0.001 (Tukey–Kramer multiple comparisons test). (I) ChIP-qPCR analysis of PRDM14, SUZ12 and H3K27me3 in wild-type and *Ctbp1/2* DKO ESCs before and after *Prdm14* induction.

DNMT3B protein level was significantly reduced in *Suz12* KO ESCs cultured in 2i plus LIF (Fig. 6D). We compared the DNMT3B protein levels in 2i plus LIF and serum plus LIF following PRDM14 induction. DNMT3B was relatively constant after *Prdm14* induction in serum plus LIF (Fig. 6E).

Next, we compared *Dnmt3a/b/l* expression between wild-type and *Ctbp1/2* DKO ESCs. The *Ctbp1/2* DKO ESC colonies were smaller than those of wild-type ESCs after three passages in 2i plus LIF (Fig. 6F) and AP activity of the *Ctbp1/2* DKO ESC colonies was very weak compared with wild-type ESCs under the 2i plus LIF condition (Fig. 6G). We isolated mRNA and proteins from *Ctbp1/2* DKO ESCs cultured in 2i plus LIF for three passages and compared *Dnmt3a/b/l* expression. The *Dnmt3b/l* repression induced by the 2i plus LIF condition was diminished in *Ctbp1/2* DKO ESCs (Fig. 6H). Therefore, CtBP1/2 is essential for transcriptional *Dnmt3b/l* repression in ground-state ESCs. As observed in *Suz12* KO ESCs, the DNMT3B protein levels were reduced in *Ctbp1/2* DKO ESCs in 2i plus LIF but not in *Ctbp1/2* DKO ESCs following PRDM14 induction in serum plus LIF (Fig. 6I,J).

Ctbp1/2 is required to maintain ground-state pluripotency

To determine the onset of *Ctbp1/2* KO ESC abnormality during the transition from serum plus LIF to 2i plus LIF, we compared the morphology of *Ctbp1/2* KO ESCs with that of wild-type ESCs every 2 days. Wild-type ESCs presented with both dome-shaped and flat colonies in serum plus LIF (Fig. 7A). At 6 days after the transfer from serum plus LIF to 2i plus LIF, the wild-type ESCs produced the dome-shaped colonies characteristic of ground-state pluripotency. In contrast, at 6 days after transfer from serum plus LIF to 2i plus LIF, the *Ctbp1/2* DKO ESCs failed to form the clear dome-shaped morphology indicative of ground-state pluripotency. The growth of *Ctbp1/2* DKO ESCs was slower than that of wild-type ESCs at 4–6 days after transfer from S serum plus LIF to 2i plus LIF (Fig. 7B). Apoptosis had slightly increased and the proportion of cells in S-phase was significantly reduced in *Ctbp1/2* DKO ESCs relative to wild-type ESCs at 4 days after transfer to 2i plus LIF (Fig. 7C,D).

DISCUSSION

Prdm14 regulates pluripotent and primordial germ cells in mice via target gene-dependent transcriptional activation and repression (Okashita et al., 2016; Nakaki et al., 2013; Yamaji et al., 2013). To understand the transcriptional activity switching mechanism in the PRDM14 complex, we performed a proteomics analysis of the PRDM14 complex in ESCs. We identified CtBP1/2 as a critical component of PRDM14-mediated transcriptional repression. The repressive marker of histone modification H3K27me3 was enriched near the PRDM14 and CtBP2 co-occupied regions in mESCs. CtBP1/2 was required to increase SUZ12 and H3K27me3 binding at the repressive PRDM14 targets. Thus, PRDM14 establishes the transcriptional networks for pluripotency mediated by recruiting the CtBP1/2–PRC2 complex.

In mice, *Prdm14* is activated in most proximal epiblast cells to induce primordial germ cell (PGC) formation (Yamaji et al., 2008; Nakaki et al., 2013). Our previous study showed that PRDM14 regulates transcriptional activation and repression in a target gene-dependent manner (Okashita et al., 2016). Our MS analysis identified the molecules involved in transcriptional activation, including the esBAF complex (Ho et al., 2009b) and those participating in transcriptional repression including the NODE complex (Liang et al., 2008). These components of the PRDM14 complex are evidence that PRDM14 switches its transcriptional activity by forming various complexes depending on the target genes involved. CBFA2T2 is a core partner of PRDM14 and essential for PRDM14-mediated transcriptional activation and repression (Nady et al., 2015; Tu et al., 2016). PRDM14 co-evolved with CBFA2T2 during deuterostome evolution, which strongly suggests the functional dependence of PRDM14 on CBFA2T2 (Kawaguchi et al., 2019). The nervy homology 2 domain (NHR2) of CBFA2T2 participates in homotypic and heterotypic oligomerization, and this domain might serve as an interaction surface for the partner molecules of PRDM14. Our data showed that the loss of *Cbfa2t2* diminished the interaction between PRDM14 and CtBP2 in mESCs, which clearly supports the idea that a CBFA2T2 oligomer acts as an interaction surface for the PRDM14 complex.

Conflicting results for the interaction between PRDM14 and PRC2 have been reported (Tu et al., 2016; Nady et al., 2015; Yamaji et al., 2013). Here, we found that shortly after PRDM14 expression was induced, the SUZ12 and H3K27me3 levels were significantly increased at the repressive PRDM14 target genes. We also showed that SUZ12 interacts with both PRDM14 and CtBP2 in mESC. Our knockout studies clearly provide evidence that PRDM14 recruits the PRC2 complex through CBFA2T2 and CtBP1/2 at the repressive PRDM14 complex targets. This discovery may resolve the discrepancy of the previous study concerning the interaction between the PRDM14 and PRC2 complexes.

Global DNA methylation decreases during the transition from metastable- to ground-state pluripotency associated with transcriptional repression of *Dnmt3a/b/l* upon upregulation of *Prdm14* (Habibi et al., 2013; Yamaji et al., 2013). Here, although transcriptional *Dnmt3b/l* repression was significantly diminished, its protein levels were reduced in *Suz12* KO and *Ctbp1/2* DKO ESCs under the 2i plus LIF condition. These findings indicate post-transcriptional DNMT3A/B regulation in ground-state ESCs. Consistent with our results, *Prdm14* upregulation in 2i plus LIF conditions induces ubiquitin-dependent DNMT3A/B degradation (Sim et al., 2017). PRDM14 forms a ternary complex with G9A (also known as EHMT2) and DNMT3A/B. G9A-mediated lysine methylation of DNMT3A/B triggers ubiquitin-dependent protein

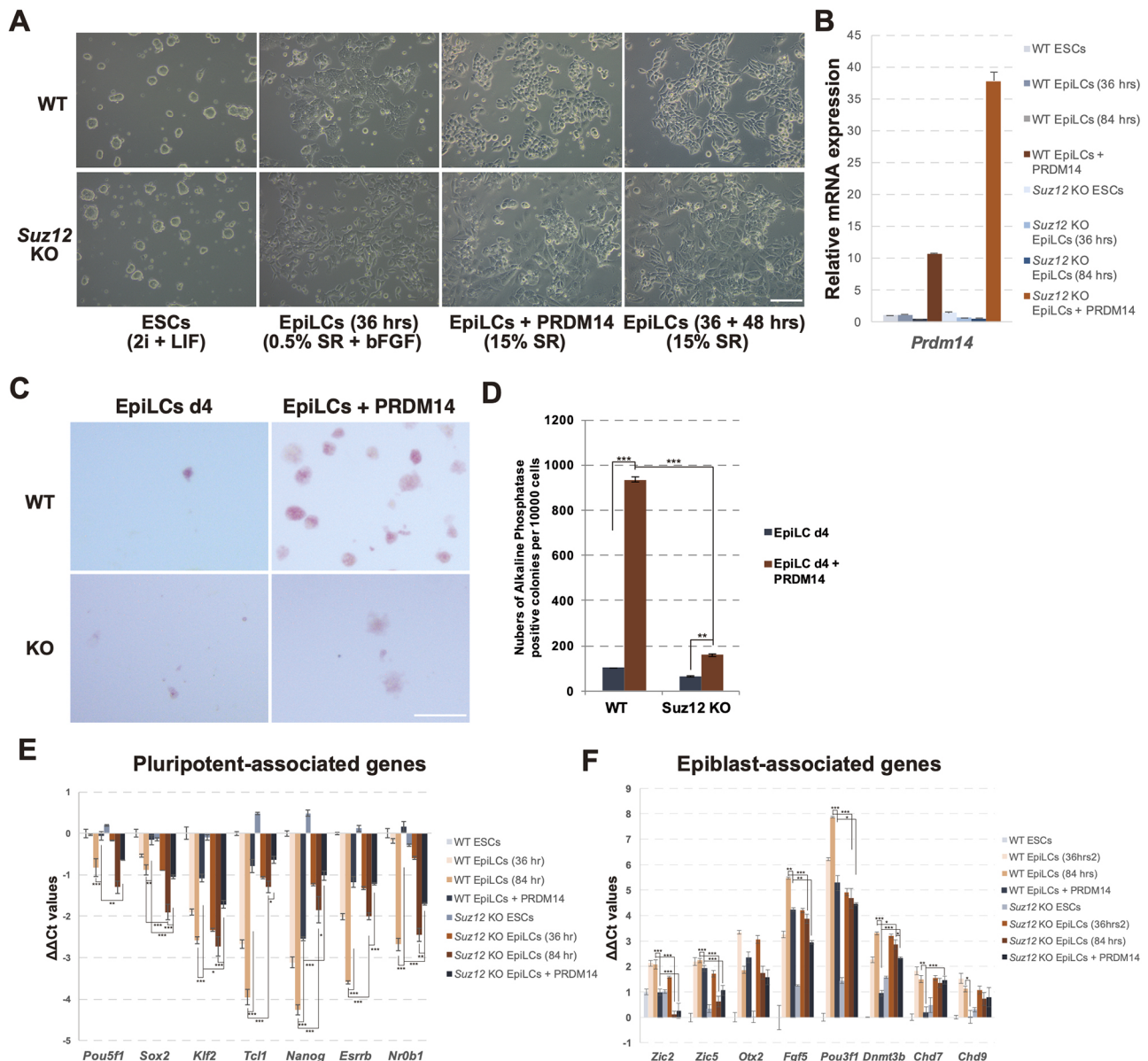


Fig. 5. *Suz12* is required for PRDM14-mediated transition from primed to naïve pluripotency. (A) Morphology of wild-type (WT), *Suz12* KO ESCs and EpiLCs before and after *Prdm14* induction. Results are representative of two experiments. (B) qRT-PCR of *Prdm14* in wild-type and *Suz12* KO ESCs and EpiLCs before and after *Prdm14* induction. Results are mean \pm s.e.m. of biological triplicates. (C,D) AP staining of EpiLCs derived from wild-type and *Suz12* KO ESCs before and after *Prdm14* induction (C). (D) Quantitative analysis of experiments in C. Results are mean \pm s.e.m. of biological triplicates. *** P <0.001 (Tukey–Kramer multiple comparisons test). (E,F) qRT-PCR of indicated genes in wild-type and *Suz12* KO ESCs, and EpiLCs before and after *Prdm14* induction. Results are mean \pm s.e.m. of biological triplicates. * P <0.05, ** P <0.01, *** P <0.001 (Tukey–Kramer multiple comparisons test).

degradation. In this study, DNMT3B protein levels were relatively stable after *Prdm14* induction in *Suz12* and *Ctbp1/2* DKO ESCs under the serum plus LIF condition. Therefore, ubiquitin-dependent DNMT3A/B protein degradation is controlled by both PRDM14 induction and 2i. Our MS analysis of PRDM14 did not find G9A or DNMT3B in serum plus LIF. The interactions of PRDM14 with G9A and DNMT3B might be enhanced by 2i, which governs ubiquitin-dependent DNMT3A/B protein degradation in ground-state ESCs.

We discovered that CtBP1/2 maintains ground-state pluripotency. As *Prdm14*-deficient ESCs can be expanded in 2i plus LIF (Yamaji et al., 2013), the function of CtBP1/2 in ground-state pluripotency maintenance is independent of that of PRDM14. The phenotype of *Ctbp1/2* DKO in ground-state ESCs resembles that of *Klf2* KO ESCs cultured in 2i (Yeo et al., 2014). There was an abnormal upregulation

of PGC markers in *Klf2* KO ESCs under 2i conditions. In contrast, the expression of PGC-markers in *Ctbp1/2* DKO ESCs were similar to those in wild-type ESCs under the 2i plus LIF condition (data not shown). These observations imply that the molecular pathways responsible for ESC abnormality under 2i conditions can be distinguished between *Klf2* KO and *Ctbp1/2* DKO. The mechanistic insight for the abnormality of ground-state pluripotency caused by the loss of *Ctbp1/2* DKO warrants further investigation.

Here, we established that the target-dependent transcriptional activity of PRDM14 is defined by the partner switching in the re-establishment of transcription factor network for naïve pluripotency. Further study will be needed to unravel the mechanism of PRDM14 complex target-dependent gene recognition.

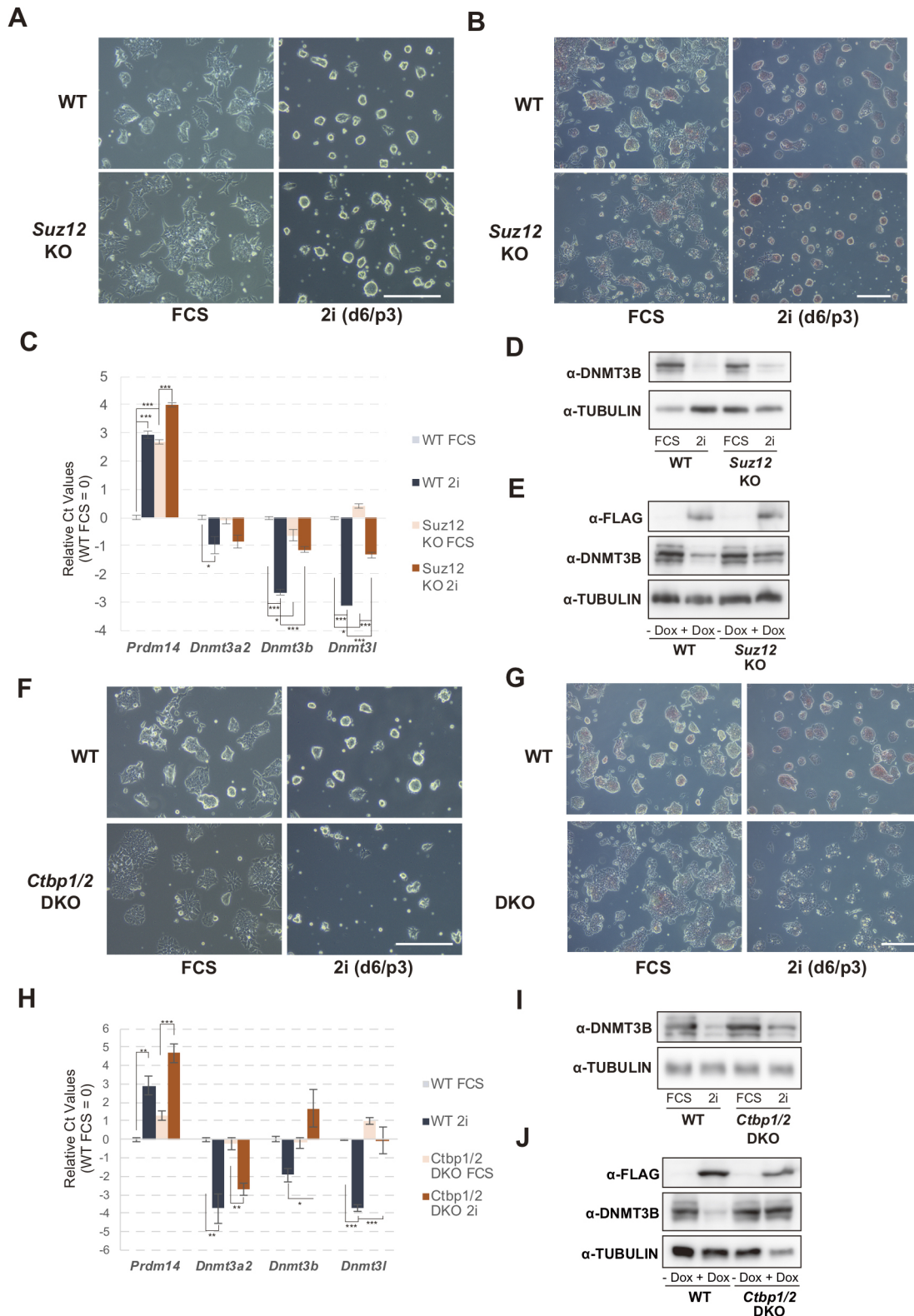


Fig. 6. See next page for legend.

MATERIALS AND METHODS

Cell culture

E14tg2a ESCs (RIKEN Cell Bank) were cultured in Glasgow minimum essential medium (GMEM; Wako Pure Chemical Industries, Ltd, Osaka, Japan) containing 10% fetal calf serum (FCS; Invitrogen, Carlsbad, CA,

USA), 1 mM glutamine (Wako Pure Chemical Industries, Ltd), nonessential amino acids (Wako Pure Chemical Industries, Ltd) and 0.1 mM 2-mercaptoethanol (Wako Pure Chemical Industries, Ltd). The culture was supplemented with 1000 U/ml of leukemia inhibitory factor (LIF; Wako Pure Chemical Industries, Ltd) in the absence of feeder cells. ESCs were

Fig. 6. The CtBP1/2-PRC2 axis is required for transcriptional *Dnmt3b/l* repression during transition from metastable- to ground-state pluripotency.

(A) Morphology of wild-type and *Suz12* KO ESCs in serum plus LIF (FCS) or 2i plus LIF [d6/p3, days (d) and passage (p) numbers after the transfer from serum plus LIF to 2i plus LIF]. Scale bar: 50 μ m. (B) AP staining of wild-type (WT) and *Suz12* KO ESCs under serum plus LIF or 2i plus LIF condition. Scale bar: 50 μ m. (C) qRT-PCR of indicated genes in wild-type and *Suz12* KO ESCs in serum plus LIF or 2i plus LIF. Results are mean \pm s.e.m. of biological triplicates. * P <0.05, *** P <0.001 (Tukey–Kramer multiple comparisons test). (D) Western blot of indicated proteins in wild-type and *Suz12* KO ESCs in serum plus LIF or 2i plus LIF. (E) Western blot of indicated proteins in wild-type and *Ctbp1/2* DKO ESCs before and after *Prdm14* induction. (F) Morphology of wild-type and *Ctbp1/2* DKO ESCs in serum plus LIF or 2i plus LIF. Scale bar: 50 μ m. (G) AP staining of wild-type and *Ctbp1/2* DKO ESCs under serum plus LIF or 2i plus LIF conditions. Scale bar: 50 μ m. (H) qRT-PCR of indicated genes in wild-type and *Ctbp1/2* DKO ESCs in serum plus LIF or 2i plus LIF. Results are mean \pm s.e.m. of biological triplicates. * P <0.05, ** P <0.01, *** P <0.001 (Tukey–Kramer multiple comparisons test). (I) Western blot of indicated proteins in wild-type and *Ctbp1/2* DKO ESCs in serum plus LIF or 2i plus LIF. (J) Western blot of indicated proteins in wild-type and *Ctbp1/2* DKO ESCs before and after *Prdm14* induction. Results in A,B,D–G,I,J are representative of two experiments.

cultured in N2B27 medium with 2i (PD0325901, 0.4 μ M; WAKO Pure Chemical Industries, Ltd; CHIR99021, 3 μ M; Sigma-Aldrich, St Louis, USA) (Hayashi et al., 2011).

Induction of EpiLCs

ESCs were cultured in N2B27 medium with 3 μ M CHIR99021 (Sigma-Aldrich, St Louis, USA), 0.4 μ M PD0325901 (Wako Pure

Chemical Industries, Ltd) and LIF on a dish coated with 0.01% (w/v) poly-L-ornithine (Millipore EMD, Billerica, MA, USA) and 10 ng ml⁻¹ laminin (BD Bioscience). EpiLC induction was performed as previously described, with minor modifications (Hayashi et al., 2011). EpiLCs were induced from ESCs in N2B27 basal medium containing 20 ng ml⁻¹ activin A (PeproTech, London, UK) and 0.1% (w/v) StemSure[®] Serum replacement (SR) (Wako Pure Chemical Industries, Ltd) for 3 days on a dish coated with 16.7 μ g ml⁻¹ human plasma fibronectin (Millipore EMD). After EpiLC induction, the cells were collected and replated with or without doxycycline in GK15 medium on a dish coated with 16.7 μ g ml⁻¹ human plasma fibronectin (Millipore EMD). For the colony formation assay of AP-positive cells, ESCs, EpiLCs and EpiLCs with or without PRDM14 were dissociated by use of TrypLE Select (Invitrogen). Cells (10⁴) were cultured under standard ESC culture conditions. After culturing for 3 days, the cells were stained for AP activity.

Generation of knockout ESCs using a CRISPR-Cas9 system

Guide RNAs for *Cbfa2t2*, *Suz12* and *CtBP1/2* were generated in pX330-U6-Chimeric_BB-CBh-hSpCas9 (Addgene plasmid #42230; deposited by Feng Zhang; Cong et al., 2013). The guide RNA sequences are listed in Table S1. The pX330 was co-transfected with pCAG-EGFP into induced PRDM14 ESCs (Okashita et al., 2016). The GFP-positive fraction was sorted by Cell Sorter (No. SH800; Sony Biotechnology, Inc., Tokyo, Japan). Genomic DNA deletions were sequenced and lack of protein expression was confirmed by western blotting.

Immunoprecipitation and western blotting

Cells were lysed in immunoprecipitation buffer [50 mM Tris-HCl pH 8.0, 150 mM NaCl, 1% (w/v) NP40, and 0.1% (w/v) Triton X-100]. Lysates

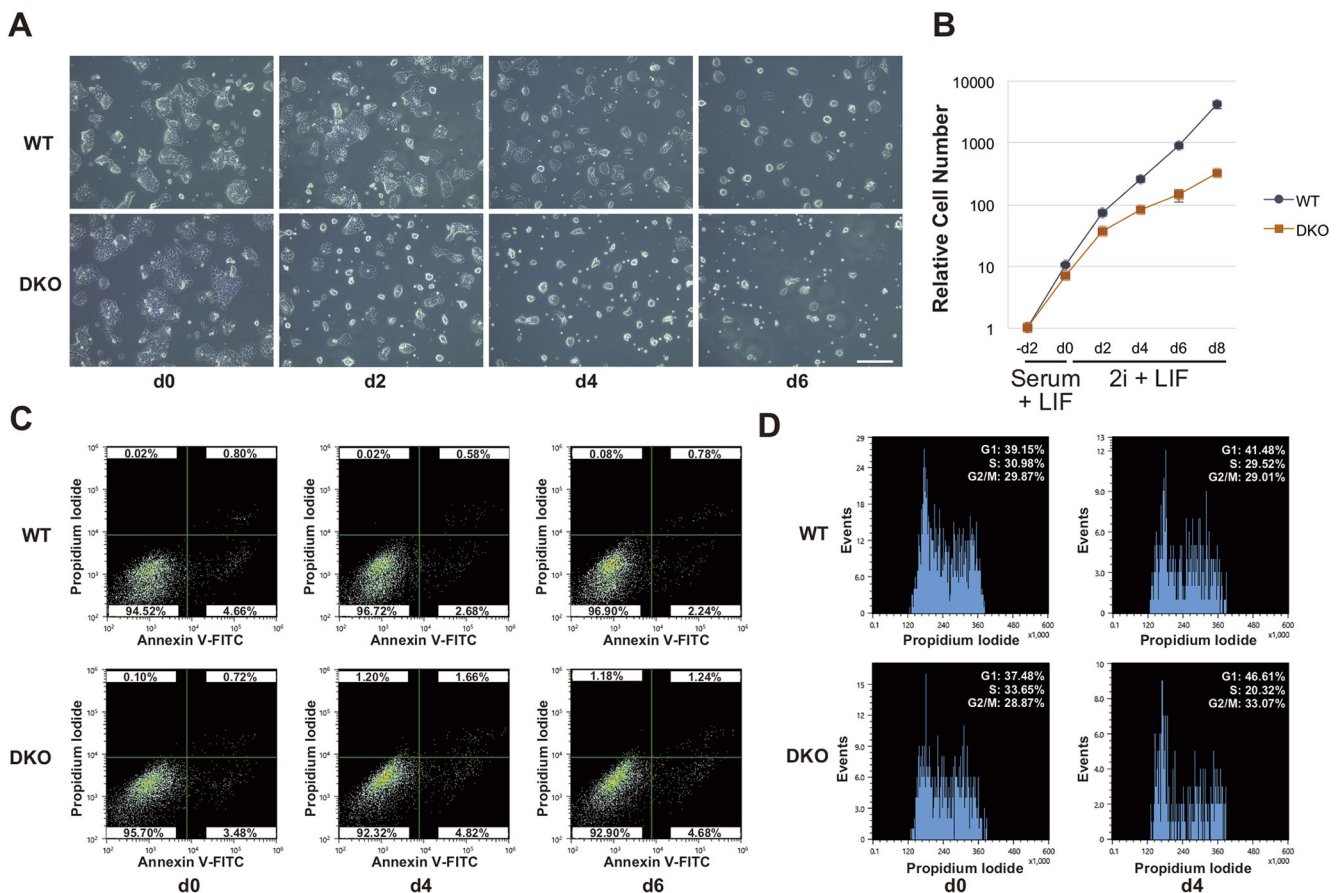


Fig. 7. *Ctbp1/2* is required to maintain ground-state pluripotency. (A) Morphology of wild-type (WT) and *Ctbp1/2* DKO ESCs during transition from metastable- to ground-state pluripotency. The cells were transferred into 2i plus LIF at d0 (from serum plus LIF) and analyzed at day 2, 4 and 6 (d2, d4, d6). (B) Growth curves of wild-type and *Ctbp1/2* DKO ESCs during transition from metastable- to ground-state pluripotency. (C) Apoptotic cells were monitored by propidium iodide and annexin V double staining. (D) Cell cycle distribution of wild-type and *Ctbp1/2* DKO ESCs in serum plus LIF 4 days after transfer from serum plus LIF to 2i plus LIF. Results are representative of two experiments.

were incubated with anti-FLAG- or anti-CtBP2 antibody, captured with protein G or protein A magnetic beads (Bio-Rad Laboratories, Hercules, USA). Protein complexes were washed three times with a buffer composed of 50 mM Tris-HCl pH 8.0, 5 M NaCl, and 0.1% (w/v) NP40 and eluted with glycine buffer (pH 2.0). Immunoprecipitants were denatured with 2-mercaptoethanol, separated on polyacrylamide-SDS gels, and blotted on polyvinylidene fluoride (PVDF) membranes. Proteins on the membranes were probed using the following primary antibodies: anti-FLAG (Sigma-Aldrich; F1804, 1:500), anti-CBFA2T2 (Bethyl Laboratories, Inc.; A303-593A, 1:500), anti-CtBP2 (BD Biosciences; 612044, 1:1000), anti-BRG1 (Merck Millipore; 07-478, 1:1000), anti-DDB1 (Abcam; ab109027, 1:500), anti-CUL4B (Proteintech; 12916-1-AP, 1:1000), anti-PRMT5 (Merck Millipore; 07-405, 1:1000) and anti-MOV10 (Proteintech; 10307-1-AP, 1:1000) antibodies. The membranes were incubated with horseradish peroxidase-coupled secondary antibodies. All antibodies were detected with Immunostar LD (Wako Pure Chemical Industries, Ltd).

In vitro protein synthesis and pulldown assay

FLAG-PRDM14 and HA-TET2 proteins were synthesized by means of the Human Cell-Free Protein Expression System (Takara Bio Inc., Shiga, Japan) according to the manufacturer's instructions. FLAG-PRDM14 and HA-TET2 were incubated in a binding buffer (20 mM Tris-HCl pH 8.0, 100 mM KCl, 5 mM MgCl₂, 2 mM DTT, 0.1% Triton X-100, 1 mM PMSF) at 4°C for 3 h. The mixture was incubated with rat anti-HA antibody (Roche, 3F10) and captured with protein G magnetic beads, followed by western blotting with anti-FLAG antibody.

Protein identification by mass spectrometry

The immunoprecipitated proteins were separated on a polyacrylamide-SDS gel and stained with Silver Stain for Mass Spectrometry (Thermo Fisher Scientific, Waltham, MA). For the in-gel digestion of proteins, each lane was excised into 13–14 gel slices and the slices cut into ~1-mm pieces. Proteins in the gel pieces were reduced with DTT (Thermo Fisher Scientific), alkylated with iodoacetamide (Thermo Fisher Scientific), and digested with trypsin (Promega, Madison, WI, USA) or Trypsin/Lys-C Mix, Mass Spec Grad (Promega) in a buffer containing 40 mM ammonium bicarbonate (pH 8.0) overnight at 37°C. The resultant peptides were analyzed on an Advance UHPLC system (AMR, Tokyo, Japan) coupled to a Q Exactive mass spectrometer (Thermo Fisher Scientific) and the raw mass spectrum processed using Xcalibur (Thermo Fisher Scientific). The raw LC-MS/MS data was analyzed against the SwissProt database or the NCBI nonredundant protein database restricted to *Mus musculus* using Proteome Discoverer version 1.4 (Thermo Fisher Scientific) with the Mascot search engine version 2.4 (Matrix Science, London, UK). A decoy database comprised of either randomized or reversed sequences in the target database was used for false discovery rate (FDR) estimation, and the Percolator algorithm (Kall et al., 2007) was used to evaluate false positives. Search results were filtered against 1% global FDR for high confidence level.

ChIP and sequential ChIP

Cells were cross-linked with 1% (w/v) paraformaldehyde for 10 min at room temperature. Cross-linked cells were lysed with SDS buffer. Cross-linked DNA–protein complexes were sheared in a Covaris M220 system (Covaris Instruments). DNA–protein complexes were incubated with anti-FLAG, anti-CtBP2, anti-HDAC1 (Abcam; ab46985), anti-TET1 (Merck Millipore; 09-872), anti-TET2 (Abcam; 124297), and anti-H3KAc (Merck Millipore; 06-599) antibodies at 4°C for 12 h. The antibody–protein–DNA complexes were collected by use of protein A or protein G SureBeads (Bio-Rad Laboratories). De-fixed DNA was purified by phenol/chloroform extraction and precipitated with ethanol. For re-ChIP analysis, the antibody–protein–DNA complexes were recovered with TE buffer (10 mM Tris-HCl pH 8.0, 1 mM EDTA) containing 20 mM DL-dithiothreitol (DTT) and followed by a second immunoprecipitation. Enrichment of the proteins on the genome was analyzed by qPCR using the primers listed in Table S1.

Microarray and data analyses

Total RNA was purified with a PureLink™ RNA Mini Kit (Ambion, Inc.). Purified total RNA (150 ng) was labeled with a GeneChip™ WT PLUS

reagent kit (Thermo Fisher Scientific) and hybridized to a GeneChip™ Mouse Gene 2.1 ST array strip (Thermo Fisher Scientific) according to the manufacturer's instructions. The CELL files of the GenChIP data were normalized by robust multi-array average (RMA) at the default setting in Affymetrix Expression Console™ (Thermo Fisher Scientific). Expression data were visualized with R software and Cluster 3.0 software. Data has been deposited in the GEO databases under accession number GSE134666.

Immunofluorescence analysis

Cells were treated with PBS containing 0.5% Triton-X to permeabilize. Permeabilized cells were incubated with primary antibody solution containing anti-OCT4 antibody (Santa Cruz Biotechnology, Inc. Sc-8628; 1/500) or anti-NANOG antibody (eBioscience™, 14-5761-80, 1:500), and followed by a Alexa 555 anti-mouse-IgG (abcam, ab150106; 1:500) or DyLight anti-rat IgG (ROCKLAND, 612-142-120; 1:500) secondary antibody reaction.

Analysis of apoptotic cells and cell cycle distribution

To detect apoptotic cells, wild-type and *Ctbp1/2* DKO ESCs cultured in serum LIF or 2i plus LIF were stained with FITC-conjugated annexin V and propidium iodide (PI) according to the manufacturer's protocol (Nacalai Tesque, Kyoto, Japan). Cell cycle distributions were determined by PI staining followed by flow cytometry (Seki et al., 2007).

Acknowledgements

We would like to thank all members of the Seki laboratory for stimulating discussion.

Competing interests

The authors declare no competing or financial interests.

Author contributions

Conceptualization: Y. Seki; Validation: Y. Suwa, Y. Seki; Investigation: M.Y., Y. Suwa, K.S., N.O., N.T., M.K., K.M., A.N., Y. Seki; Writing - original draft: Y. Seki; Writing - review & editing: K.M., A.N., Y. Seki; Visualization: M.Y., Y. Suwa, K.S., N.O., Y. Seki; Supervision: Y. Seki; Project administration: Y. Seki; Funding acquisition: Y. Seki.

Funding

This study was supported by a Grant-in-Aid for Young Scientists (A) (Japan Society for the Promotion of Science KAKENHI grant number 24681040), a Grant-in-Aid for Scientific Research (B) (Japan Society for the Promotion of Science KAKENHI grant number 18H02422), the Promotion of Joint International Research (Japan Society for the Promotion of Science KAKENHI grant number 15KK0262), the Scientific Research on Innovative Areas, 'Epigenome dynamics and regulation in germ cells' (Ministry of Education, Culture, Sports, Science, and Technology KAKENHI grant numbers 26112514 and 16H01223), the Scientific Research on Innovative Areas, 'Mechanisms regulating gamete formation in animals' (Ministry of Education, Culture, Sports, Science, and Technology KAKENHI grant number 16H01258), and the Scientific Research on Innovative Areas, 'Program of totipotency: From decoding to designing' (Ministry of Education, Culture, Sports, Science, and Technology KAKENHI grant number 20H05375). This work was supported by the program of the Joint Usage/Research Center for Developmental Medicine, Institute of Molecular Embryology and Genetics of Kumamoto University.

Data availability

Microarray data has been deposited in Gene Expression Omnibus (GSE134666). Mass spectrometry data has been deposited in ProteomeXchange (PXD020571).

Supplementary information

Supplementary information available online at <https://jcs.biologists.org/lookup/doi/10.1242/jcs.240176.supplemental>

Peer review history

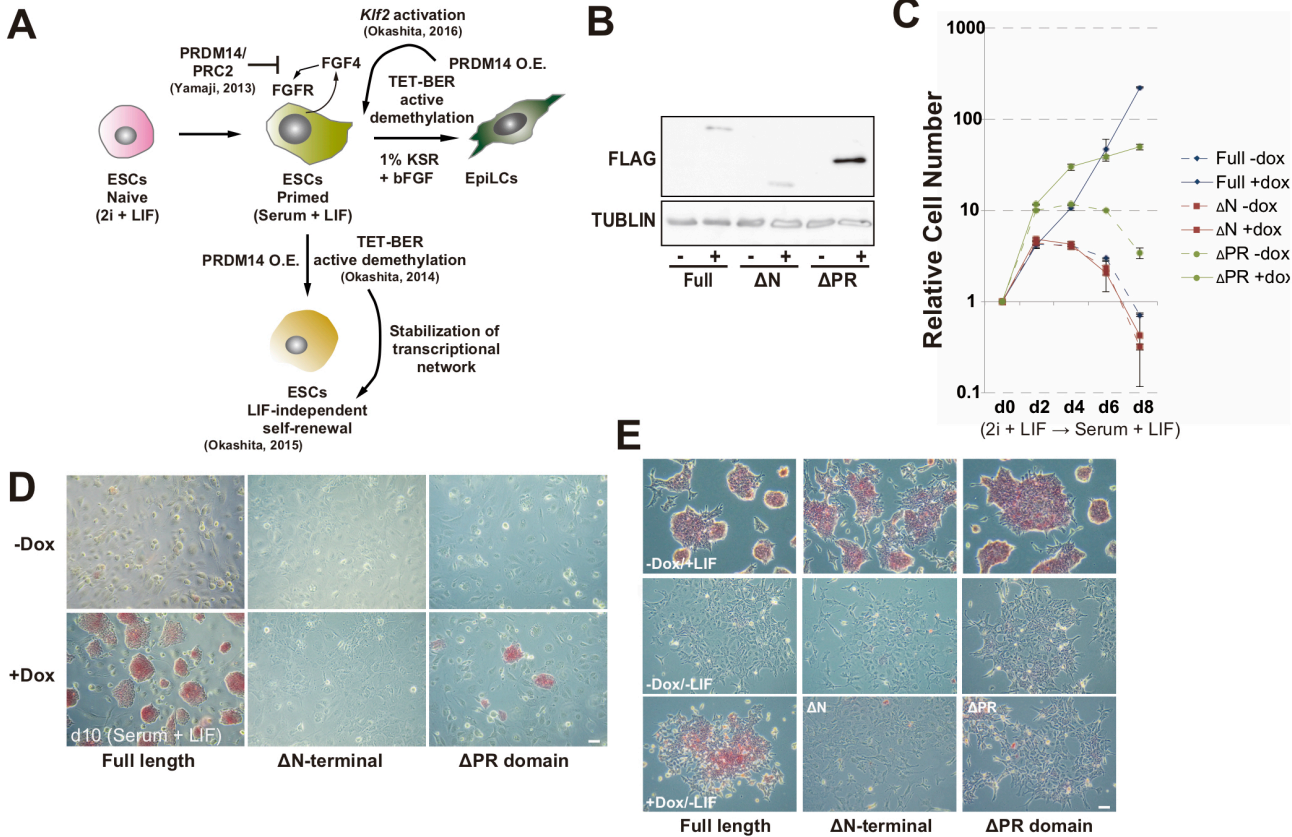
The peer review history is available online at <https://jcs.biologists.org/lookup/doi/10.1242/jcs.240176.reviewer-comments.pdf>

References

Cong, L., Ran, F. A., Cox, D., Lin, S., Barretto, R., Habib, N., Hsu, P. D., Wu, X., Jiang, W., Marraffini, L. A. et al. (2013). Multiplex genome engineering using CRISPR/Cas systems. *Science* **339**, 819–823. doi:10.1126/science.1231143

- Gao, J., Buckley, S. M., Cimmino, L., Guillamot, M., Strikoudis, A., Cang, Y., Goff, S. P. and Aifantis, I. (2015). The CUL4-DDB1 ubiquitin ligase complex controls adult and embryonic stem cell differentiation and homeostasis. *Elife* **4**, e07539. doi:10.7554/eLife.07539.018
- Habibi, E., Brinkman, A. B., Arand, J., Kroeze, L. I., Kerstens, H. H., Matarese, F., Lepikhov, K., Gut, M., Brun-Heath, I., Hubner, N. C. et al. (2013). Whole-genome bisulfite sequencing of two distinct interconvertible DNA methylomes of mouse embryonic stem cells. *Cell Stem Cell* **13**, 360-369. doi:10.1016/j.stem.2013.06.002
- Hayashi, K., Ohta, H., Kurimoto, K., Aramaki, S. and Saitou, M. (2011). Reconstitution of the mouse germ cell specification pathway in culture by pluripotent stem cells. *Cell* **146**, 519-532. doi:10.1016/j.cell.2011.06.052
- Ho, L., Jothi, R., Ronan, J. L., Cui, K., Zhao, K. and Crabtree, G. R. (2009a). An embryonic stem cell chromatin remodeling complex, esBAF, is an essential component of the core pluripotency transcriptional network. *Proc. Natl. Acad. Sci. USA* **106**, 5187-5191. doi:10.1073/pnas.0812888106
- Ho, L., Ronan, J. L., Wu, J., Staahl, B. T., Chen, L., Kuo, A., Lessard, J., Nesvizhskii, A. I., Ranish, J. and Crabtree, G. R. (2009b). An embryonic stem cell chromatin remodeling complex, esBAF, is essential for embryonic stem cell self-renewal and pluripotency. *Proc. Natl. Acad. Sci. USA* **106**, 5181-5186. doi:10.1073/pnas.0812889106
- Ji, X., Dadon, D. B., Abraham, D. B., Lee, T. I., Jaenisch, R., Bradner, J. E. and Young, R. A. (2015). Chromatin proteomic profiling reveals novel proteins associated with histone-marked genomic regions. *Proc. Natl. Acad. Sci. USA* **112**, 3841-3846. doi:10.1073/pnas.1502971112
- Kagiyama, S., Kurimoto, K., Hirota, T., Yamaji, M. and Saitou, M. (2013). Replication-coupled passive DNA demethylation for the erasure of genome imprints in mice. *EMBO J.* **32**, 340-353. doi:10.1038/emboj.2012.331
- Kall, L., Canterbury, J. D., Weston, J., Noble, W. S. and MacCoss, M. J. (2007). Semi-supervised learning for peptide identification from shotgun proteomics datasets. *Nature Meth.* **4**, 923-925. doi:10.1038/nmeth1113
- Kawaguchi, M., Sugiyama, K., Matsubara, K., Lin, C.-Y., Kuraku, S., Hashimoto, S., Suwa, Y., Yong, L. W., Takino, K., Higashida, S. et al. (2019). Co-option of the PRDM14-CBFA2T complex from motor neurons to pluripotent cells during vertebrate evolution. *Development* **146**. doi:10.1242/dev.168633
- Kim, T. W., Kang, B.-H., Jang, H., Kwak, S., Shin, J., Kim, H., Lee, S.-E., Lee, S.-M., Lee, J.-H., Kim, J.-H. et al. (2015). Ctbp2 modulates NuRD-mediated deacetylation of H3K27 and facilitates PRC2-mediated H3K27me3 in active embryonic stem cell genes during exit from pluripotency. *Stem Cells* **33**, 2442-2455. doi:10.1002/stem.2046
- Kurimoto, K., Yamaji, M., Seki, Y. and Saitou, M. (2008). Specification of the germ cell lineage in mice: a process orchestrated by the PR-domain proteins, Blimp1 and Prdm14. *Cell Cycle* **7**, 3514-3518. doi:10.4161/cc.7.22.6979
- Liang, J., Wan, M., Zhang, Y., Gu, P., Xin, H., Jung, S. Y., Qin, J., Wong, J., Cooney, A. J., Liu, D. et al. (2008). Nanog and Oct4 associate with unique transcriptional repression complexes in embryonic stem cells. *Nat. Cell Biol.* **10**, 731-739. doi:10.1038/ncb1736
- Ma, Z., Swigut, T., Valouev, A., Rada-Iglesias, A. and Wysocka, J. (2011). Sequence-specific regulator Prdm14 safeguards mouse ESCs from entering extraembryonic endoderm fates. *Nat. Struct. Mol. Biol.* **18**, 120-127. doi:10.1038/nsmb.2000
- Nady, N., Gupta, A., Ma, Z., Swigut, T., Koide, A., Koide, S. and Wysocka, J. (2015). ETO family protein Mtgr1 mediates Prdm14 functions in stem cell maintenance and primordial germ cell formation. *Elife* **4**, e10150. doi:10.7554/eLife.10150
- Nakaki, F., Hayashi, K., Ohta, H., Kurimoto, K., Yabuta, Y. and Saitou, M. (2013). Induction of mouse germ-cell fate by transcription factors in vitro. *Nature* **501**, 222-226. doi:10.1038/nature12417
- Niwa, H. (2014). The pluripotency transcription factor network at work in reprogramming. *Curr. Opin. Genet. Dev.* **28**, 25-31. doi:10.1016/j.gde.2014.08.004
- Ohno, R., Nakayama, M., Naruse, C., Okashita, N., Takano, O., Tachibana, M., Asano, M., Saitou, M. and Seki, Y. (2013). A replication-dependent passive mechanism modulates DNA demethylation in mouse primordial germ cells. *Development* **140**, 2892-2903. doi:10.1242/dev.093229
- Okashita, N., Kumaki, Y., Ebi, K., Nishi, M., Okamoto, Y., Nakayama, M., Hashimoto, S., Nakamura, T., Sugawara, K., Kojima, N. et al. (2014). PRDM14 promotes active DNA demethylation through the ten-eleven translocation (TET)-mediated base excision repair pathway in embryonic stem cells. *Development* **141**, 269-280. doi:10.1242/dev.099622
- Okashita, N., Sakashita, N., Ito, K., Mitsuya, A., Suwa, Y. and Seki, Y. (2015). PRDM14 maintains pluripotency of embryonic stem cells through TET-mediated active DNA demethylation. *Biochem. Biophys. Res. Commun.* **466**, 138-145. doi:10.1016/j.bbrc.2015.08.122
- Okashita, N., Suwa, Y., Nishimura, O., Sakashita, N., Kadota, M., Nagamatsu, G., Kawaguchi, M., Kashida, H., Nakajima, A., Tachibana, M. et al. (2016). PRDM14 drives OCT3/4 recruitment via active demethylation in the transition from primed to naive pluripotency. *Stem Cell Rep.* **7**, 1072-1086. doi:10.1016/j.stemcr.2016.10.007
- Seki, Y. (2018). PRDM14 is a unique epigenetic regulator stabilizing transcriptional networks for pluripotency. *Front. Cell Dev. Biol.* **6**, 12. doi:10.3389/fcell.2018.00012
- Seki, Y., Yamaji, M., Yabuta, Y., Sano, M., Shigeta, M., Matsui, Y., Saga, Y., Tachibana, M., Shinkai, Y. and Saitou, M. (2007). Cellular dynamics associated with the genome-wide epigenetic reprogramming in migrating primordial germ cells in mice. *Development* **134**, 2627-2638. doi:10.1242/dev.005611
- Sim, Y. J., Kim, M. S., Nayfeh, A., Yun, Y. J., Kim, S. J., Park, K. T., Kim, C. H. and Kim, K. S. (2017). 2iL maintains a naive ground state in ESCs through two distinct epigenetic mechanisms. *Stem Cell Rep.* **8**, 1312-1328. doi:10.1016/j.stemcr.2017.04.001
- Tu, S., Narendra, V., Yamaji, M., Vidal, S. E., Rojas, L. A., Wang, X., Kim, S. Y., Garcia, B. A., Tuschl, T., Stadtfeld, M. et al. (2016). Co-repressor CBFA2T2 regulates pluripotency and germline development. *Nature* **534**, 387-390. doi:10.1038/nature18004
- Yamaji, M., Seki, Y., Kurimoto, K., Yabuta, Y., Yuasa, M., Shigeta, M., Yamanaka, K., Ohinata, Y. and Saitou, M. (2008). Critical function of Prdm14 for the establishment of the germ cell lineage in mice. *Nat. Genet.* **40**, 1016-1022. doi:10.1038/ng.186
- Yamaji, M., Ueda, J., Hayashi, K., Ohta, H., Yabuta, Y., Kurimoto, K., Nakato, R., Yamada, Y., Shirahige, K. and Saitou, M. (2013). PRDM14 ensures naive pluripotency through dual regulation of signaling and epigenetic pathways in mouse embryonic stem cells. *Cell Stem Cell* **12**, 368-382. doi:10.1016/j.stem.2012.12.012
- Yeo, J. C., Jiang, J., Tan, Z. Y., Yim, G. R., Ng, J. H., Goke, J., Kraus, P., Liang, H., Gonzales, K. A., Chong, H. C. et al. (2014). Klf2 is an essential factor that sustains ground state pluripotency. *Cell Stem Cell* **14**, 864-872. doi:10.1016/j.stem.2014.04.015

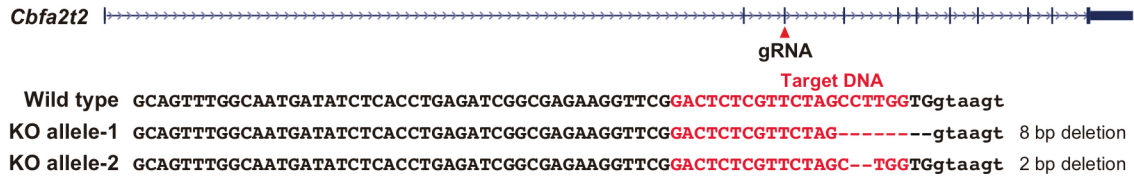
Supplementary Figure 1



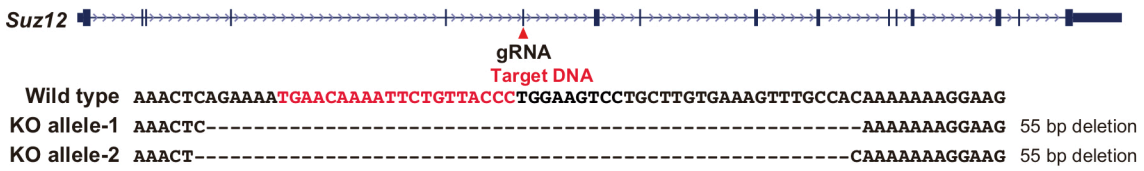
Supplementary Figure 1. (A) The scheme of the PRDM14 function in the maintenance and induction of pluripotency. (B) The establishment of *Prdm14*-inducible ESCs lacking endogenous *Prdm14*. (C) The proliferation rate of *Prdm14*-deficient ESCs with or without exogenous *Prdm14* in serum plus LIF condition. Error bars indicate \pm standard errors of the mean (SEM) of biological triplicates. (D) Alkaline phosphatase staining of *Prdm14*-deficient ESCs with or without exogenous *Prdm14* ten days after the transfer to serum plus LIF condition. (E) Alkaline phosphatase staining of ESCs with or without exogenous *Prdm14* expression in serum plus LIF or serum minus LIF. Scale bar : 50 μ m

Supplementary Figure 2

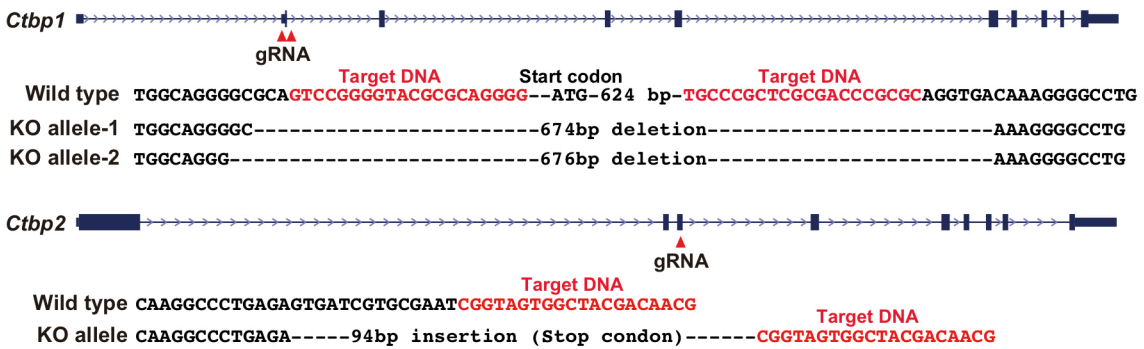
A



B



C



Supplementary Figure 2. The deletion sequence of *Cbfa2t2*, *Suz12* and *Ctbp1/2* locus by CRISPR/Cas9 system.

Table S1. Oligonucleotide lists for guide RNAs, qRT-PCR, Hpa II -qPCR and ChIP-qPC Guide RNA

Gene	Strand	Sequence(5'-3')
<i>Ctbp1</i> upstream	Forward	CACCGTCCGGGGTACGCGCAGGGG
	Reverse	AAACCCCCTGCGCGTACCCCGGAC
<i>Ctbp1</i> downstream	Forward	CACCGTGCCCGCTCGCGACCCGCGC
	Reverse	AAACGCGCGGGTTCGCGAGCGGGCAC
<i>Ctbp2</i>	Forward	CACCGATCCGCCCCAGCTGATGAA
	Reverse	AAACTTCATCAGCTGGGGGCGGATC
<i>Cbfa2t2</i>	Forward	CACCGACTCTCGTTCTAGCCTTGG
	Reverse	AAACCCAAGGCTAGAACGAGAGTC
<i>Suz12</i>	Forward	CACCGTGAACAAAATTCTGTTACCC
	Reverse	AAACGGGTAACAGAATTTTGTTCAC

ChIP-qPCR

Gene	Strand	Sequence(5'-3')
<i>Dnmt3b</i> (-7.5 kb)	Forward	GGGGGAATTACTTTGCCGGAG
	Reverse	TGCAATTCTCTATGGGGTTCG
<i>Dnmt3b</i> (-6.2 kb)	Forward	TCTTACCTCGGCTGGGAGAA
	Reverse	ACGAAGCTGAGAAGTTAGACCT
<i>Zfp281</i>	Forward	CATAGCCTGATGGAACCATTG
	Reverse	ATGTACGTTCTGCCCGTGAG
<i>Id1</i>	Forward	TGCAGATGGACCTGCTAAGTG
	Reverse	TCTCACACACAAACCCCTGTC
<i>Tcl1</i>	Forward	GCCCTGAGTGCAAACCTTACAG
	Reverse	CTATGTGGTGTGGGAAAGC
<i>Dppa3</i>	Forward	CCTCGTGTGAGAATTTGCATC
	Reverse	GCCACGGCTATTCTATTCAAGT
<i>Tfap2c</i>	Forward	TCTAAAAAGCCCCTTGTGGAG
	Reverse	GACAGAGCCTCCAGAGAAAG

qRT-PCR

Gene	Strand	Sequence(5'-3')
<i>Prdm14</i> CDS	Forward	TGTGGTACGGAAATGGCTATG
	Reverse	AAACACCTTTCCACAGCGTTC
<i>Prdm14</i> 3'UTR	Forward	GGAATCCATTTCAGACCAGGAG
	Reverse	GCACATAGTCGCTGGCTACAG
<i>Dnmt3b</i>	Forward	CTCGCAAGGTGTGGGCTTTTGTAA
	Reverse	CTGGGCATCTGTCATCTTTCACC
<i>Dnmt3l</i>	Forward	CCAGGGCAGATTTCTTCTAAGGTC
	Reverse	TGAGCTGCACAGAGGCATCC
<i>Gja1</i>	Forward	GTGCAAGTGTGTAAGCGTGTG
	Reverse	CACAAAGATCCATGAGGAAG

<i>Tfap2c</i>	Forward	ACGCGGAAGAGTATGTTGTTG
	Reverse	TTGTATGTTCCGGCTCCAAGAC
<i>Dppa3</i>	Forward	AGGCTCGAAGGAAATGAGTTTG
	Reverse	TCCTAATTCTTCCCGATTTTCG
<i>Sox15</i>	Forward	TCCCCTTACCTATCCCCAGAC
	Reverse	AGTGTGCATTCTGGTTCCTTG
<i>Mok</i>	Forward	GGAGAAGACACCCATTATCAGAGA
	Reverse	GATATTCTCCGGCTTCACGTC
<i>Rbbp7</i>	Forward	GGGACCTGCGTAATCTGAAACT
	Reverse	GCGCATCAGTACCACTTGAGG
<i>Lefty2</i>	Forward	CAAAACACCCGGGACTCTTAGG
	Reverse	TAAATGACATGGGCAAAGCTG
<i>Meis2</i>	Forward	AAGGCGCTTGCTCCTATCTC
	Reverse	TGGTTGTCAAAACACCATTCC
<i>Zic2</i>	Forward	AACTTCCCTAGCCCACTTTCC
	Reverse	TCCGGGAGTTTACAAATGGAC
<i>Zic5</i>	Forward	CTGAAGTCATGCGGACGATAC
	Reverse	CTAATTAGACCCGGTGGCAAG
<i>Uhrf1</i>	Forward	GCCACTTCTTCACTCCTCACC
	Reverse	CACATCTCAGCCTTCCATGAC
<i>Rhox6</i>	Forward	TTTCCAAGAGACTCGTACCC
	Reverse	GTTTCGAGAACATCAGCACTC
<i>Nanos3</i>	Forward	AATCCTCTGCAGCTCCTGAAC
	Reverse	CACACATAATCCCGCAAATG
<i>Chd9</i>	Forward	TAGATTGATTGGGGGAAGGTG
	Reverse	AAGTGGGACTGCATTGACTTG
<i>Uhrf1</i>	Forward	GCCACTTCTTCACTCCTCACC
	Reverse	CACATCTCAGCCTTCCATGAC
<i>Id1</i>	Forward	CAACAGAGCCTCACCTCTC
	Reverse	AGAAATCCGAGAAGCACGAA
<i>Pou5f1</i>	Forward	CTCTCCCATGCATTCAAACCTG
	Reverse	CCCCTGTTGTGCTTTTAATCC
<i>Sox2</i>	Forward	CTTGCTGGGTTTTGATTCTGC
	Reverse	AAGACCACGAAAACGGTCTTG
<i>Klf2</i>	Forward	CCCAGGAAAGAAGACAGGAG
	Reverse	AGGCATTTCTCACAAGGCATC
<i>Tcl1</i>	Forward	GAACTTGCCTTCTTCTCACG
	Reverse	TCACAGGTCAGGTGGGTACAG
<i>Nanog</i>	Forward	AGCCAGGTTCTTCTTCTTC
	Reverse	AAGATCTGACGCCCTTCTTG
<i>Esrrb</i>	Forward	CGTGTGACAAGGAGACAGGAG
	Reverse	TCCAGCCACAACGTCATTATC
<i>Nr0b1</i>	Forward	GAAAGCGGTCGTAGCTGTAGG

	Reverse	GAAGCCAGTATGGAGCAGAGG
<i>Otx2</i>	Forward	GAGGTGATCCGGTGTTTTAGC
	Reverse	AATCAGTCGCACAATCCACAC
<i>Fgf5</i>	Forward	ATGAGTGCATCTGCTCTGCTC
	Reverse	CGTCTGTGGTTTCTGTTGAGG
<i>Pou3f1</i>	Forward	ATTTATTCGTGGAGCCTCTCG
	Reverse	TATACACAGATGCGGCTCTCG
<i>Chd7</i>	Forward	CGAGGAGAACCTGGACAAGAC
	Reverse	CTTTCAGTGGAAGTCTGCTG